

Rotationally induced fingering patterns in a two-dimensional heterogeneous porous mediumChing-Yao Chen^{*} and Ting-Shiang Lin*Department of Mechanical Engineering, National Chiao Tung University, Hsinchu, Taiwan, 30010, Republic of China*José A. Miranda[†]*Departamento de Física, Universidade Federal de Pernambuco, Recife, Pernambuco 50670-901, Brazil*

(Received 26 July 2016; published 4 November 2016)

Rotating fluid flows under two-dimensional homogeneous porous media conditions (or in a rotating Hele-Shaw cell) reveal the development of complex interfacial fingering patterns. These pattern-forming structures are characterized by the occurrence of finger competition events, finger pinch-off episodes, as well as by the production of satellite droplets. In this work, we use intensive numerical simulations to investigate how these fully nonlinear pattern growth phenomena are altered by the presence of permeability heterogeneities in the rotating porous medium. This is done by employing a diffuse-interface Darcy-Cahn-Hilliard description of the problem and considering a permeability field presenting a log-Gaussian distribution, characterized by a variance s and a correlation length l . We study how the heterogeneity measures s and l couple to the governing hydrodynamic dimensionless parameters of the problem and introduce important changes on the pattern formation dynamics of the system.

DOI: [10.1103/PhysRevE.94.053105](https://doi.org/10.1103/PhysRevE.94.053105)**I. INTRODUCTION**

Viscous fingering (or Saffman-Taylor) instability [1,2] is driven by the viscosity difference between fluids. This hydrodynamic instability occurs when a less-viscous fluid pushes a more-viscous one in the effectively two-dimensional (2D) geometry of a Hele-Shaw cell, which is equivalent to a 2D homogeneous porous medium. This popular pattern-forming problem involves the development of long smooth fingers in rectangular channels or ramified fronts if the injection-driven flow takes place in an open radial geometry [3].

An alternative form of fingering instability in confined geometry arises when there exists a difference in density between the fluids. Specifically, this type of instability occurs when a fluid, surrounded by another of lower density, is located in a Hele-Shaw cell that rotates about an axis perpendicular to the cell plates [4,5]. Centrifugal forces act on the density difference between the fluids, and a morphological instability results.

Meticulous laboratory experiments and sophisticated numerical simulations reveal the outcome of a great variety of patterned shapes in this 2D homogeneous rotating environment [5–9]. These rotation-induced fingering structures are very distinct from the ones detected in viscosity-driven radial Hele-Shaw flows generated by injection. For example, instead of presenting branched, tip-split fingers as in the injection-driven radial flows, the rotating fingering patterns usually exhibit nonsplitting fingers of different lengths that compete among themselves. It has also been found that such finger competition events depend on the viscosity difference (or, on the viscosity contrast) between the fluids. Depending on the viscosity contrast, the rotationally driven fingering patterns may change from teardrop-like structures to thin filamented arms presenting swelled ends or to a backbone architecture with nearly constant finger widths. Additionally, complex

pinch-off phenomena are also detected, characterizing the formation of satellite droplets which are detached from the main body of the rotating inner fluid droplet.

Despite the importance of all the pattern-forming information extracted from the valuable studies performed in Refs. [4–9], they only explored the confined rotationally driven problem under spatially homogeneous conditions. One valid, and still open, question is to ask how the important pattern-forming behaviors observed in the system will be affected by the existence of heterogeneities in such a confined, rotating flow situation. In this work, we address this issue and analyze the development of centrifugally driven interfacial structures in a 2D rotating heterogeneous porous medium.

We tackle the problem by employing advanced numerical simulations and investigating how the interplay of centrifugal, viscous, surface tension, and heterogeneity effects influence the dynamics and morphology of the emerging fingering patterns. In particular, we are interested in examining how the heterogeneity of the confined medium affects and modifies the most relevant pattern formation mechanisms that are usually found during rotating flows in the corresponding purely homogeneous situations.

The remainder of this paper is organized as follows. The basic setup of the physical problem, the governing equations, and the numerical methods are introduced in Sec. II. Section III presents our numerical results that unveil a number of appealing rotationally induced fingered structures as the heterogeneity properties of the 2D rotating porous medium are changed. Specifically, we discuss how finger competition events, finger pinch-off episodes, and the phenomenon of satellite droplet formation are impacted by the system's permeability heterogeneity. Finally, Sec. IV summarizes our main findings and conclusions.

II. PHYSICAL PROBLEM AND GOVERNING EQUATIONS

We study the development of interfacial instabilities that arise at the interface separating two immiscible fluids in a rotating 2D heterogeneous porous medium whose permeability

^{*}chingyao@mail.nctu.edu.tw[†]jme@df.ufpe.br

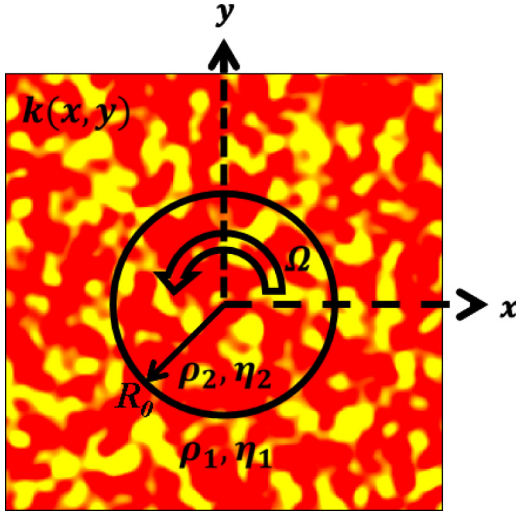


FIG. 1. Representative sketch of a rotating heterogeneous porous medium, showing a typical permeability distribution $k(x, y)$, where a clearer (darker) area corresponds to a region of higher (lower) permeability. The whole system rotates with constant angular velocity Ω . The inner fluid is more dense ($\rho_2 > \rho_1$), so the initially circular boundary of radius R_0 separating the fluids is centrifugally unstable, and deforms, to eventually produce complex interfacial patterns.

is represented by $k(x, y)$. A circular drop of the inner fluid 2, whose initial radius is denoted by R_0 , is placed in the porous medium surrounded by the outer fluid 1, as illustrated in Fig. 1. A 2D Cartesian coordinate system, whose origin is located at the center of the inner fluid drop, is defined. The densities and viscosities of the fluids are denoted by ρ_j and η_j , respectively ($j = 1, 2$). The entire system rotates with constant angular velocity Ω . We focus our attention on the centrifugally induced motion where $\rho_2 > \rho_1$.

The governing equations for this immiscible binary fluid system can be described by a diffuse-interface approach based on the Darcy-Cahn-Hilliard (equivalent to the Hele-Shaw-Cahn-Hilliard) model and are written as [9–14]

$$\nabla \cdot \mathbf{u} = 0, \quad (1)$$

$$\nabla p = -\frac{\eta}{k} \mathbf{u} + \rho r \Omega^2 \mathbf{e}_r - \epsilon \nabla \cdot [\rho (\nabla c) (\nabla c)^T], \quad (2)$$

$$\rho \left(\frac{\partial c}{\partial t} + \mathbf{u} \cdot \nabla c \right) = \alpha \nabla^2 \mu, \quad (3)$$

$$\mu = \frac{\partial f_0}{\partial c} - \frac{\epsilon}{\rho} \nabla \cdot (\rho \nabla c), \quad (4)$$

$$f_0 = f^* c^2 (1 - c)^2. \quad (5)$$

Here, \mathbf{u} denotes the velocity vector, p the pressure, η the viscosity, and ρ the density of the binary system. In addition, r is the radial distance from the origin, and \mathbf{e}_r represents the unit vector in the radial direction. The phase-field variable is represented by c , so $c = 1$ in the bulk of fluid 1, and $c = 0$ in the bulk of fluid 2. The constants ϵ and α represent the coefficient of capillarity and mobility, respectively. The chemical potential is denoted by μ , and f_0 is a free energy (or the Helmholtz free energy) with a characteristic specific energy f^* .

Equation (1) expresses the incompressibility condition, and Eq. (2) is the Darcy-Cahn-Hilliard equation. Notice that the second and third terms on the right-hand side of Eq. (2) represent the centrifugal force and the interfacial force connected to surface tension, respectively. We consider a vanishing Reynolds number situation, and the Coriolis force can be safely neglected [4,9,15,16]. Finally, Eq. (3) is a diffusion equation for the phase-field variable. From this Darcy-Cahn-Hilliard formulation [Eqs. (1)–(5)], an expression for the surface free energy existing on the interface can be calculated as [12]

$$E = \rho \int \left[f_0 + \frac{\epsilon}{2} (\nabla c)^2 \right] dV, \quad (6)$$

where V is the volume of the fluid domain.

We follow Refs. [10,11,17,18] and apply a Boussinesq approximation such that the density is represented by a constant bulk average density of the two fluids ρ_b , except in the centrifugal force term. Furthermore, to avoid discontinuity of the profiles of viscosity η and density ρ within the thin diffusive boundary region, the smooth variations that depend on the phase-field variable are assumed as

$$\eta(c) = \eta_1 \exp[R(1 - c)], \quad R = \ln\left(\frac{\eta_2}{\eta_1}\right), \quad (7)$$

$$\rho(c) = \rho_1 c + \rho_2 (1 - c). \quad (8)$$

To generate the desired statistical distribution of the permeability field, we employ an algorithm originally proposed by Shinozuka and Jan [19]. In this context, the heterogeneous permeability field $k(x, y)$ is expressed in terms of a characteristic value K , and the exponential of a random function $g(x, y)$, whose Gaussian distribution is characterized by the variance s , and the spatial correlation length l as follows [10,11,14,18]:

$$k(x, y) = K \exp[g(x, y)], \quad (9)$$

$$g(x, y) = s^2 \exp\left\{-\pi \left[\left(\frac{x}{l}\right)^2 + \left(\frac{y}{l}\right)^2 \right]\right\}, \quad (10)$$

with mean $\bar{g} = 0$, and a logarithmic mean permeability $\overline{\log[k(x, y)]} = \log[K]$. The readers are referred to Refs. [18,19] for more details about the statistical generation of the permeability patterns. Within this description, changes in the magnitude of the permeability are determined by the variance s , while the typical size of more permeable regions is prescribed by the correlation length l . For example, $l = 0.2$ (or l is 1/5 of a rescaled initial inner fluid drop radius $R_0 = 1$) in the representative permeability field illustrated in Fig. 1. Note that by considering the limit of vanishing variance in Eqs. (9) and (10), i.e., by setting $s = 0$, one reproduces the homogeneous medium situation. Notice that our present study mainly aims to identify the effects of variance and correlation length of heterogeneity in such a way that all the permeability fields associated with different correlation lengths considered in the simulations are generated by utilizing a single set of random numbers. This is particularly important for allowing more direct comparisons of situations involving different values of the correlation length. Otherwise, for totally independent realizations of the permeability field, the intrinsic random nature of their distributions would make

such a comparison very difficult. It should be noted that this approach has been successfully used by previous simulational works that examined heterogeneous injection-driven flows in rectangular and radial geometries [10,14,18]. It is also worth mentioning that good examples of real injection-driven Hele-Shaw cell experimental realizations of effectively 2D heterogeneous media include Hele-Shaw cells with random gaps [20] and with roughened glass plates [21].

At this point, it is convenient to rewrite the governing equations (1)–(5) in a dimensionless form,

$$\nabla \cdot \mathbf{u} = 0, \quad (11)$$

$$\nabla p = -\frac{\eta}{k} \mathbf{u} - \left(c + \frac{\rho_2}{\Delta\rho} \right) \mathbf{r} \mathbf{e}_r - \frac{C}{\text{Ga}} \nabla \cdot [(\nabla c)(\nabla c)^T], \quad (12)$$

$$\frac{\partial c}{\partial t} + \mathbf{u} \cdot \nabla c = \frac{1}{\text{Pe}} \nabla^2 \mu, \quad (13)$$

$$\mu = \frac{\partial f_0}{\partial c} - C \nabla^2 c, \quad (14)$$

$$f_0 = c^2(1-c)^2. \quad (15)$$

We nondimensionalized these Boussinesq Darcy-Cahn-Hilliard equations as follows. The initial radius of the inner fluid drop R_0 and density difference $\Delta\rho = \rho_2 - \rho_1$ have been taken as characteristic scales. Viscosities and time are scaled by η_1 , and $\eta_1/(\Delta\rho\Omega^2 K)$, respectively. In addition, a characteristic velocity $(\Delta\rho\Omega^2 R_0 K)/\eta_1$, the pressure $\Delta\rho\Omega^2 R_0^2$, and a specific free energy f_0^* have also been used in the nondimensionalization process. Dimensionless parameters, such as the viscosity contrast A , the rotationally modified Galileo number Ga , the Péclet number Pe , and the Cahn number C fully characterize our physical system and are defined as

$$A = \frac{e^R - 1}{e^R + 1}, \quad \text{Ga} = \frac{\Delta\rho\Omega^2 R_0^2}{\rho_b f^*},$$

$$\text{Pe} = \frac{\rho_b \Delta\rho\Omega^2 K R_0^2}{\alpha \eta_1 f^*}, \quad C = \frac{\epsilon}{f^* R_0^2}.$$

From this point on, we describe our system by using the dimensionless version of all equations.

To solve the governing equations numerically, we recast them into the well-known stream function-vorticity formulation (ϕ, ω) [22], yielding

$$u = \frac{\partial \phi}{\partial y}, \quad v = -\frac{\partial \phi}{\partial x}, \quad (16)$$

$$\nabla^2 \phi = -\omega, \quad (17)$$

where

$$\omega = -R \left(u \frac{\partial c}{\partial y} - v \frac{\partial c}{\partial x} \right) - \frac{k}{\eta} \left(y \frac{\partial c}{\partial x} - x \frac{\partial c}{\partial y} \right) - \frac{1}{k} \left(u \frac{\partial k}{\partial y} - v \frac{\partial k}{\partial x} \right) + \frac{kC}{\eta \text{Ga}} \left[\frac{\partial c}{\partial x} \left(\frac{\partial^3 c}{\partial x^2 \partial y} + \frac{\partial^3 c}{\partial y^3} \right) - \frac{\partial c}{\partial y} \left(\frac{\partial^3 c}{\partial x \partial y^2} + \frac{\partial^3 c}{\partial x^3} \right) \right].$$

To simulate the interfacial phenomena, a 4×4 computational domain, whose size is twice larger than of the initial drop diameter $D_0 = 2R_0 = 2$, is applied. For such a domain, the boundary conditions of the problem are prescribed as

$$x = \pm 2 : \phi = 0, \quad \frac{\partial c}{\partial x} = 0, \quad \frac{\partial^2 c}{\partial x^2} = 0, \quad (18)$$

$$y = \pm 2 : \phi = 0, \quad \frac{\partial c}{\partial y} = 0, \quad \frac{\partial^2 c}{\partial y^2} = 0. \quad (19)$$

To reproduce the extremely fine structures of the fingers, we apply a highly accurate pseudospectral method. As a result, the actual boundary conditions applied in the numerical code are $\partial\phi/\partial y = 0$ at $y = \pm 2$. To ensure the appropriateness of such a condition, the simulations are terminated before the outermost fingertips reach the used computational boundaries. Consequently, no concentration gradient is generated on the boundaries, and the above conditions automatically lead to $\phi = 0$. Both c and ϕ are expanded in a cosine series in the streamwise direction. In the normal direction, discretization is accomplished by a sixth-order compact finite differences. To obtain the time evolution of the interface, equations for the phase variable c , vorticity ω , and stream function ϕ are solved in sequence in a mesh of 513×513 grid points. Time integration for the phase variable equation is fully explicit, and utilizes a third-order Runge-Kutta procedure. The spatial derivatives in the phase equation are discretized by sixth- and fourth-order compact finite difference schemes for diffusion and convection terms, respectively. A dynamical time step determined by the local maximum Courant-Friedrichs-Lewy (CFL) number, i.e., $\text{CFL} = (u, v)_{\max} \frac{\Delta t}{\Delta x}$, is applied to advance in time. A small $\text{CFL} = 0.1$ is taken in the simulations. At every time step, the local maximum speed $(u, v)_{\max}$ is checked in the entire domain and then $\Delta t = 0.1 \Delta x / (u, v)_{\max}$ is obtained to advance the simulation in time. For more details about the numerical scheme, we refer the readers to Refs. [11,17,23].

Validations of the present diffuse-interface method are generally supported by the excellent qualitative and quantitative agreements with existing experimental observations, and theoretical predictions on pattern formation, as well as the number of fingers achieved in previous works on similar radial Hele-Shaw flows, e.g., rotational flows [7–9], and suction flows [13] under homogeneous conditions. In particular, the cases of low viscosity contrast when $A = 0.4$ – 0.5 in a rotating Hele-Shaw configuration simulated in Ref. [9] agree well, both qualitatively and quantitatively, with the existing experiments reported by Alvarez-Lacalle *et al.* [6,8]. These facts substantiate the validity and accuracy of the numerical scheme employed in the our current study.

III. RESULTS AND DISCUSSION

In this section, we present our numerical results and discuss, both qualitatively and quantitatively, how the heterogeneous nature of the rotating porous medium affects the fully nonlinear dynamics of the system and how it influences the advanced-time morphological properties of the emerging interfacial patterns. Since the two key parameters of the permeability field are given by the variance of the heterogeneity field s ,

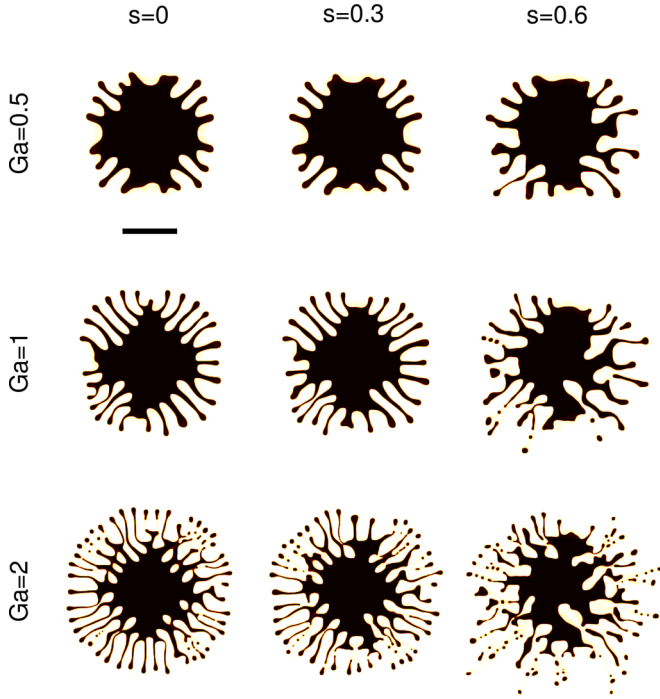


FIG. 2. Fingering patterns for $A = 0.76$ and $l = 0.2$, taken at time $t = 7$. We consider three values of the Galileo number Ga : 0.5 (top row), 1 (middle row), and 2 (bottom row). Moreover, three values of the variance s are taken: 0 (left column), 0.3 (central column), and 0.6 (right column). Recall that $s = 0$ corresponds to the homogeneous situation. The scale bar represents R_0 .

and the spatial correlation length l , for the sake of clarity and simplicity we divide our analysis into two separate parts: (i) in Sec. III A, we focus on the effects due to changes in s , while (ii) in Sec. III B we concentrate on the impact produced by changes in l . Without loss of generality, and based on the existing numerical results for flows in the homogeneous environment of a rotating Hele-Shaw cell [9,13], we take $Pe = 9 \times 10^3$ and $C = 10^{-5}$ in all the simulations shown in the rest of this investigation.

A. Influence of the variance of the heterogeneity field

We begin our discussion by analyzing Fig. 2, which focuses on a representative positive viscosity contrast case where $\eta_2 > \eta_1$, namely $A = 0.76$. The fingering patterns plotted in Fig. 2 are shown at time $t = 7$. Throughout this section, we consider a fixed value of the spatial correlation length $l = 0.2$, while the governing parameters A, Ga , and s may vary. For the particular value of the viscosity contrast used in Fig. 2 ($A = 0.76$), we have that the inner fluid is about 7.4 times more viscous than the outer fluid. Here, the major driving force is centrifugal in nature and competes with surface-tension, viscous, and heterogeneity effects. In order to search for various different morphological behaviors, in Fig. 2 we consider three values of the Galileo number Ga : 0.5 (top row), 1 (middle row), and 2 (bottom row). In addition, we consider three increasingly larger variances s : 0 (homogeneous condition, left column), 0.3 (central column), and 0.6 (right column). It should be noted that the variation of permeability for $s = 0.3$ and 0.6 range

between $0.74 \leq k \leq 1.39$ and $0.30 \leq k \leq 3.68$, respectively, with a logarithmic mean permeability $\overline{\log[k(x,y)]} = 0$.

For the homogeneous cases ($s = 0$) depicted in the left column of Fig. 2, the characteristic shapes of the patterns are consistent with similar structures previously obtained in Refs. [7–9]. By inspecting these homogeneous situations, one realizes that under higher Ga (stronger centrifugal effects or smaller surface tension), a larger number of fingers is produced, and more intense droplet emissions at the fingertips are triggered. Besides, one also verifies that finger competition (measured by finger length variability) among the outward-moving fingers of the inner (dark) fluid is not very intense. This can be seen by the fact that the fingertips of the outward-moving fingers all present similar radial distances from the center of the rotating droplet, defining a nearly circular outer boundary. On the other hand, the inward-moving fingers of the penetrating outer (clear) fluid that move toward the origin compete quite strongly among themselves, acquiring different lengths. These two distinct finger competition behaviors revealed by outward- and inward-moving fingers are also in line with existing laboratory experiments [6] and other numerical simulations [7–9].

If the environment is now heterogeneous, as in the cases depicted in the central ($s = 0.3$) and right ($s = 0.6$) columns of Fig. 2, then different morphological features can be identified in the fingering patterns. First, one notices that the presence of permeability heterogeneity tends to reduce the number of produced fingers. While in the homogeneous case centrifugal forces induce the fingers to evolve preferentially in the radial direction, the randomly distributed permeability field weakens such radial preference for finger growth. This favors finger merging at very early time, so the number of fully developed fingers can be reduced. This enhanced finger merging phenomenon at early times of the dynamics also explains the fact that the roots of the fully developed fingers under heterogeneous conditions appear thicker than the ones of their homogeneous counterparts.

A second relevant aspect that can be extracted from the central ($s = 0.3$) and right ($s = 0.6$) columns of Fig. 2 refers to the influence of permeability heterogeneity on the finger competition mechanism. One observes that, in such cases, finger competition of inward-moving fingers tends to increase, with the stronger penetration of a few dominant fingers of the outer fluid. Most interestingly, one can see that, under heterogeneous conditions, finger competition also arises among the outward-moving fingers of the inner fluid. This can be verified by the more evident variations in the radial positions of the outermost fingertips. This enhancement of finger competition is somewhat expected, since now fingers tend to move toward regions associated with higher permeability. As a result, the development of individual fingers is affected by the local distribution of permeability, leading to an increased finger length variability.

Still regarding the central ($s = 0.3$) and right ($s = 0.6$) columns of Fig. 2, it is also worth pointing out the impact of permeability heterogeneity on the process of finger pinch-off, as well as on the occurrence of droplet emissions near the fingertips of outward-moving fingers. The process of droplet emission under a homogeneous condition ($s = 0$) is mainly an aftermath effect of the competition between surface tension

and rotationally induced finger stretching. If, on one hand, stronger surface tension tends to prevent the occurrence of droplet emission, then, on the other hand, stronger centrifugal effects favor the increased stretching of the fingered filaments. If the local net centrifugal force within a finger exceeds the constraint of surface tension, then there is fluid accumulation at the fingertips, and satellite droplets may develop. The presence of a high permeability region accelerates the outward movement of nearby fingers, and the difference among their lengths tend to increase. These longer fingers are subjected to stronger variations of centrifugal forces, resulting in more intense droplet emissions.

Another contributing factor to cause droplet emission in a heterogeneous condition can be attributed to the action of the local tangential velocity. Even though the dominant fingering effects are driven by the radial centrifugal force, significant tangential flows could be induced by the randomly distributed permeability field. These tangential flows can break the thin fingers apart and form separate segments. A similar effect that is responsible for enhanced droplet emissions at fingertips has been observed in a rotating drop subjected to significant Coriolis force, in which case tangential flows are also relevant [9]. Nevertheless, it should be pointed out that the present tangential flow induced by permeability heterogeneity differs from the situation involving Coriolis force, mainly with respect to the locations of the pinch-off events along the fingers. While the finger pinch-off caused by the effects of the Coriolis force mostly occurs at the fingertips, the current finger pinch-off events induced by the permeability heterogeneity are not limited to these locations. This way, the presence of tiny droplets or small finger segments can also be observed at locations closer to the origin, which usually leads to the formation of an array of multiple droplets or small finger segments, instead of a single finger, as shown in Fig. 2 in the case where $Ga = 2$ and $s = 0.6$.

One additional remark about Fig. 2 is the fact that an increase in the permeability heterogeneity leads to enhanced destabilization and faster finger growth. As a matter of fact, the increment of length of the outermost finger is potentially important to the so-called breakthrough time or contaminated area in many relevant practical applications of this problem [23–25]. Finally, notice that the droplet emission and the finger pinch-off phenomena revealed in Fig. 2 are accompanied by a severe inward motion of the outer fluid fingers, something that provokes an increased fragmentation of the rotating droplet for larger values of s and Ga .

Now we turn our attention to another important physical situation, namely the zero viscosity contrast case $A = 0$, in which the rotating fluids have the same viscosity ($\eta_1 = \eta_2$). Here our main task is to understand how permeability heterogeneity influences interfacial pattern formation under such a viscosity-matched situation. This is done in Fig. 3, in which, with the exception of A , we use the same physical parameters and initial conditions as those used in Fig. 2. It is well known that the viscosity contrast plays an important role in the pattern formation process that arises in a rotating homogeneous porous medium (or Hele-Shaw cell) [7–9]. The homogeneous situation ($s = 0$) corresponding to the viscosity-matched case is depicted in the left column of Fig. 3. Compared with the corresponding cases for positive viscosity

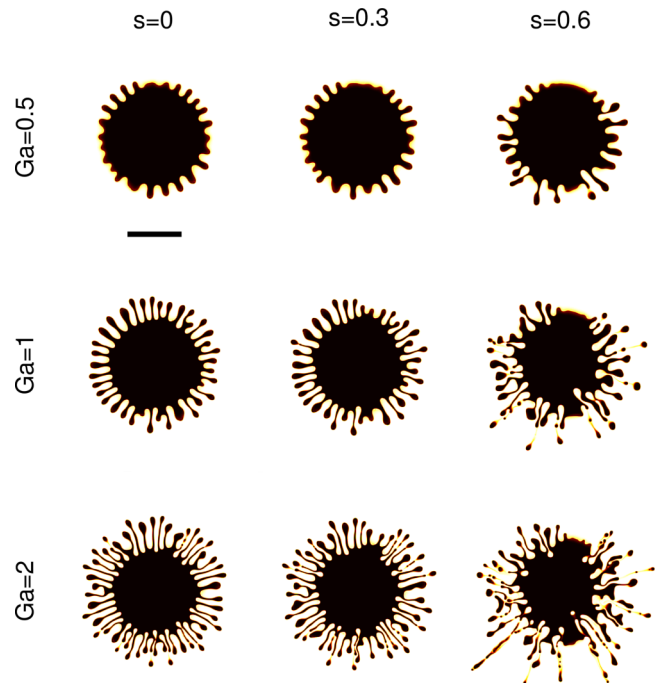


FIG. 3. Fingering patterns for $A = 0$ and $l = 0.2$, taken at time $t = 1.7$. We consider three values of the Galileo number Ga : 0.5 (top row), 1 (middle row), and 2 (bottom row). Moreover, three values of the variance s are taken: 0 (left column), 0.3 (central column), and 0.6 (right column). Note that $s = 0$ corresponds to the homogeneous situation. The scale bar represents R_0 .

contrast $A = 0.76$ shown in the left column of Fig. 2 taken at time $t = 7$, we notice that fingers develop much faster when $A = 0$. In addition, for $A = 0$, one observes weaker finger competition among outward as well as among inward-moving fingers. This happens because in the case $A = 0$ there is no preferential flow direction regarding the viscosities of the inner or outer fluids. These observations for the homogeneous case in Fig. 3 agree well with similar findings already reported in the literature [7–9].

However, if the effects of permeability heterogeneity are taken into account, different pattern-forming scenarios arise. These still unexplored behaviors are illustrated in the central ($s = 0.3$) and right ($s = 0.6$) columns of Fig. 3. One evident difference revealed by these heterogeneous cases is the fact that finger competition (of both outward- and inward-moving fingers) is enhanced. In addition, one can also see that the thicknesses of individual fingers are not uniform, and multiple slim fingers go through a pinch-off process, where droplet emissions are also detected for higher values of s and Ga . These qualitative influences of heterogeneity for $A = 0$ in Fig. 3 are consonant with the ones discussed in the positive viscosity contrast cases shown in Fig. 2, although the overall appearance of the patterns for $A = 0$ is still considerably distinct from those illustrated in Fig. 2 for $A = 0.76$.

Also notice that, in comparison with the $A = 0.76$ case, some of the effects due to permeability heterogeneity become milder in the $A = 0$ situation. For example, the penetration of the inward-moving fingers of the outer fluid is less vigorous, so the central (bulk) region of the inner droplet is relatively well

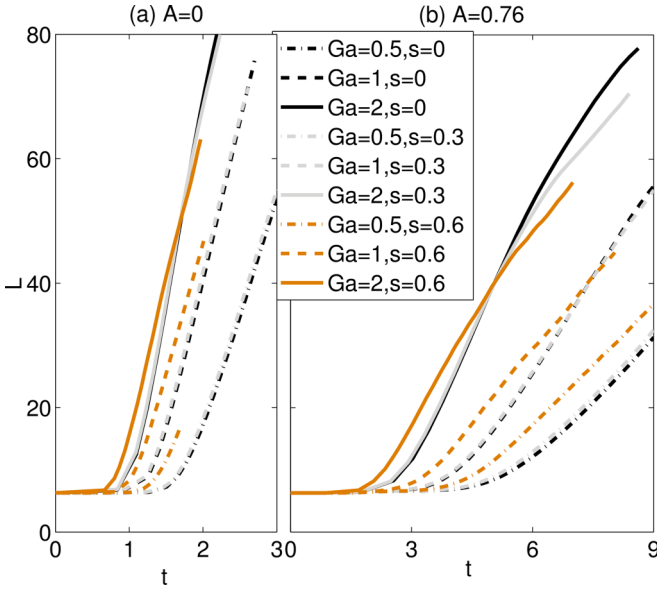


FIG. 4. Time evolution of the interfacial length L for different values of Ga and s and for $l = 0.2$. This is considered for (a) $A = 0$ (cases depicted in Fig. 3) and (b) $A = 0.76$ (situations shown in Fig. 2).

preserved and less fragmented. Moreover, the outward-moving fingers remain slim, similar to the cases under a homogeneous condition. At this point, it should be stressed that, even though they are not presented in this paper, we have verified that the general trends related to the heterogeneous nature of the medium discussed in Fig. 2 and Fig. 3 also hold for the cases of negative viscosity contrast (i.e., when $\eta_1 > \eta_2$).

In order to have a more quantitative assessment of the impact of permeability heterogeneity on the dynamics and morphology of the interfacial fingering patterns illustrated in Figs. 2 and 3, we investigate the time evolution of two useful quantities: (i) the interfacial length and (ii) the maximum finger penetration. While the interfacial length considers the evolution of all the fingers induced by rotation, expressing the total perimeter of all structures formed, the maximum finger penetration gives information about the radial mass distribution. The time evolution of the interfacial length L , for the various cases considered in Figs. 2 and 3, is displayed in Fig. 4.

For the case of a homogeneous rotating porous medium (or rotating Hele-Shaw cell) where $s = 0$, it is well established that more intense fingering occurs for larger values of Ga , a situation that is associated with earlier finger growth and with the development of longer interfacial lengths. In general, this basic trend also holds for heterogeneous situations. Nonetheless, by inspecting Fig. 4(a) and Fig. 4(b), one observes something interesting, namely the crossing of some of the curves when one increases the value of s , while Ga and l are held fixed. This fact can be clearly observed for the cases in which $Ga = 2$ for both $A = 0$ and $A = 0.76$. Such crossings do not occur in the usual homogeneous situation.

An explanation for the peculiar curve crossings shown in Fig. 4 when permeability heterogeneity is taken into account can be given as follows. First, let us define the latency time [6]

as the largest time for which the interface shape remains circular, with length $L = 2\pi$. After this time, the instability sets in, and the deformed pattern develops. So, usually we see that L remains constant until the latency time and then increases abruptly as the instability grows. By examining Fig. 4, we deduce that the shortest latency time occurs for the most heterogeneous condition $s = 0.6$. This is not surprising since heterogeneity generates stronger interfacial perturbation, causing early onset of the fingering instability. However, despite the earliest growth of the interfacial length, its average growth rate is not the largest, so after a period of time, the interfacial length for $s = 0.6$ becomes smaller than the ones associated with lower heterogeneities.

The behavior for the time evolution of L described above for $s \neq 0$ differs from the conventional findings encountered under homogeneous conditions for which $s = 0$. In the homogeneous case, a more unstable situation would form initial fingers more rapidly, leading to more prominent growth driven by centrifugal forces. As a result, an earlier growth of the interfacial length can always be associated with a larger growth rate, so either criterion can be used to describe a more unstable fingering situation. These considerations are no longer appropriate for our current heterogeneous cases. As mentioned earlier in this work, even though early fingering formation in the most heterogeneous condition is expected, the strong local permeability heterogeneity also causes severe tangential motion of the initial fingers, resulting in significant finger merging. This merging phenomenon may reduce the number of fingers significantly. Consequently, only a few fingers are able to grow further, and the total interfacial length ends up being smaller. Therefore, the earlier growth, accompanied with a lower growth rate, observed for the cases with stronger heterogeneity, explains the unconventional curve crossings detected in Fig. 4.

Another measure of interest that also quantifies the effects of permeability heterogeneities is the distance of maximum penetration of fingers r_f , involving both the inward- and outward-moving fingers. A region beyond such typical distances characterizes a contamination free area. In other words, beyond this region, a fluid (that can be either fluid 1 or fluid 2 in our two-fluid system) is not contaminated with the other fluid. Notice that the measurement of r_f includes both continuous fingers and separated droplets. The time evolution of the positions of the outermost and innermost fingertips, r_f , is depicted in Fig. 5 for the cases $A = 0$ and $A = 0.76$. The data presented in Fig. 5 agree qualitatively with similar findings reported for homogeneous rotating Hele-Shaw flows [7–9], in which faster and longer finger penetrations are observed for the cases with lower A and larger Ga . It can also be verified that if the permeability is heterogeneous, then the finger penetration events are significantly strengthened. This is in accordance with the observations made for the patterns shown in Figs. 2 and 3. More intense finger competition that takes place under heterogeneous conditions, triggers rapid growth of both inward- and outward-moving fingers, so the positions of the innermost and outermost fingertips are further away from the original interface (identified in Fig. 5 by $r_f = 1$ at $t = 0$). Incidentally, one can also observe that enhanced finger penetration occurs preferentially for lower values of the viscosity contrast, e.g., for $A = 0$.

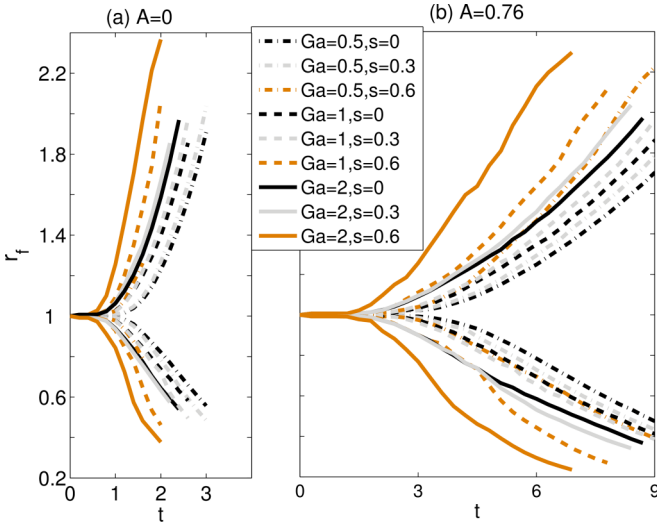


FIG. 5. Radial positions of the outermost and innermost fingertips r_f for different values of Ga and s and for $l = 0.2$. This is done for (a) $A = 0$ (cases depicted in Fig. 3) and (b) $A = 0.76$ (situations shown in Fig. 2).

Still examining Fig. 5, one can see that, while the increments of the inward and outward penetration distances under the presence of heterogeneity, e.g., for $s = 0.6$, appear nearly the same for the case in which $A = 0.76$ [Fig. 5(b)], for the $A = 0$ case [Fig. 5(a)] the outward increment is significantly larger than its inward counterpart. This more expressive outward penetration for lower values of the viscosity contrast is a result of the coupling between the effects of fluid mobility and medium permeability. Since the outward fingers are driven by the centrifugal force, they are always more active than their inward-moving analogs. These outward fingers are more mobile in the cases of lower viscosity contrast, so they are directed much more vigorously toward the area with higher permeability. Consequently, few salient fingers are formed, such as the long slim outward ones at the lower left corner for the situation in which $Ga = 2$ and $s = 0.6$ shown in Fig. 3. This exemplifies the relevance of the coupling between permeability and different viscosity contrast conditions in determining basic pattern-forming behaviors in our system.

B. Impact of the spatial correlation length

In this section, we aim attention at the spatial correlation length l and examine its role in determining the behavior of the rotating patterns. To begin understanding the influence of l , in Fig. 6 we display fingering patterns (left column), and streamlines superimposed on the permeability distributions (right column), for two representative cases in which $l = 0.08$ (top row) and $l = 0.4$ (bottom row). As mentioned earlier in this work, the value of l is related to the typical sizes of the individual clearer and darker areas that appear in the representation of the permeability distributions, i.e., low (high) values of l correspond to small (large) areas. By the way, in the permeability distributions illustrated in the right column of Fig. 6, the clearer areas are regions of higher permeability, while the darker spots characterize areas of lower permeability. Other relevant physical parameters utilized in Fig. 6 are

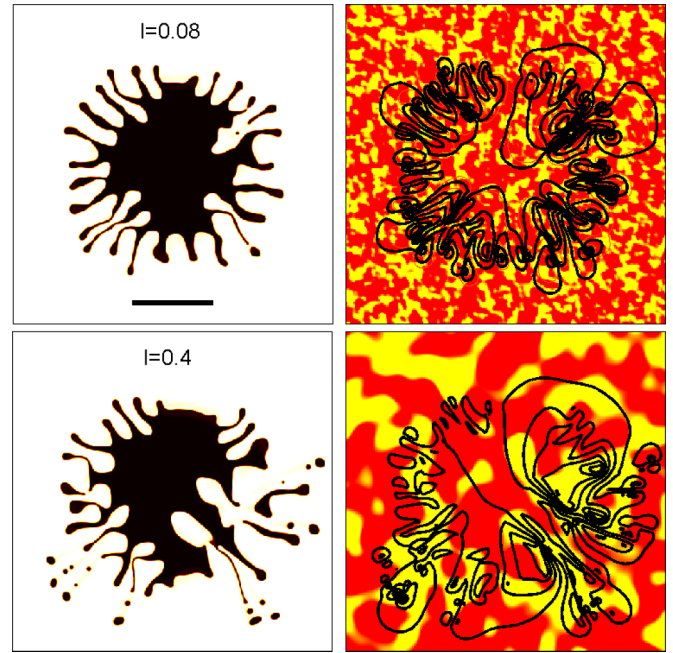


FIG. 6. Fingering patterns (left column) and streamlines superimposed on permeability distributions (right column) at $t = 6.5$ for $A = 0.76$, $Ga = 1$, and $s = 0.6$. Top row: $l = 0.08$; bottom row: $l = 0.4$. The scale bar represents R_0 .

$A = 0.76$, $Ga = 1$, and $s = 0.6$. Additionally, these images are plotted at time $t = 6.5$. It is also worth mentioning that the streamlines shown in Fig. 6 are instantaneous (taken at $t = 6.5$), continuous across the interface, and relate to both fluids. These facts can be justified as follows. Under the conditions of our rotationally induced flow problem, fluid motion takes place mainly on the interface, where fingers are driven by local vortices. In addition, in the context of our diffuse-interface method, such an interface is smooth, and presents a finite thickness, so the streamlines are indeed continuous across the fluid-fluid boundary. In this sense, the streamlines depicted in Fig. 6 represent the motion of the whole two-fluid system.

By observing the patterns illustrated in Fig. 6, one notices that an important effect of the correlation length is the way it affects the typical size of the resulting fingering structures. This can be observed by comparing the patterns exhibited in Fig. 6 for $l = 0.08$ and $l = 0.4$ with those depicted in the middle row in Fig. 2, which have been obtained by using similar parameters but for an intermediate value of the correlation length $l = 0.2$. Larger values of l induce the thinning of the branching fingers and produce the thickening of the finger basis (i.e., finger roots). In addition, one can see that there is a preferred direction for finger growth toward the bulk region having higher permeability. This can be verified by inspecting the lower-right orientation in the case of $l = 0.4$, something that can be also realized by examining the streamlines. As a consequence, fewer fully developed fingers with more rapid growth evolve for larger correlation lengths. The latter is compatible with the so-called channeling effect reported in injection-driven viscous fingering flows under heterogeneous conditions [10,11,14].

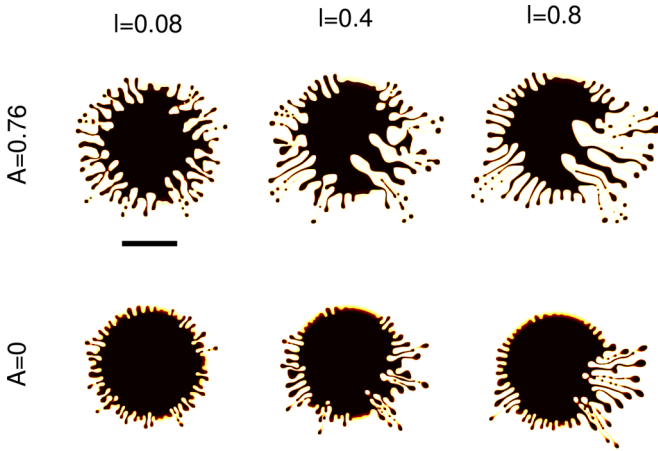


FIG. 7. Fingering patterns for $Ga = 2$ and $s = 0.6$. Top row: $A = 0.76$ at $t = 7$; bottom row: $A = 0$ at $t = 1.2$. We consider three values of the spatial correlation length l : 0.08 (left column), 0.4 (central column), and 0.8 (right column). The scale bar represents R_0 .

To further elucidate the influence of the correlation length l on the patterns' shapes, in Fig. 7 we plot fingering structures obtained for three increasingly larger values of l : 0.08 (left column), 0.4 (central column), and 0.8 (right column). To facilitate visualization of the induced effects, and to produce more intense fingering instabilities, we consider that $Ga = 2$ and $s = 0.6$. This is done for following values of the viscosity contrast A and simulation times t : $A = 0.76$ at $t = 7$ (top row) and $A = 0$ at $t = 1.2$ (bottom row). Of course, these patterns can also be compared to the intermediate correlation length cases ($l = 0.2$) shown in Figs. 2 and 3.

We first analyze the series of patterns in the top row of Fig. 7, obtained for $A = 0.76$. It is evident that larger correlation lengths tend to induce the formation of longer fingers. While the sizes of the outward pointing fingers on the left front of the patterns remain comparable for all correlation lengths, the lengths of the penetrating inward-moving fingers tend to increase for larger values of l . For instance, in the cases with $l = 0.4$ and 0.8 , two predominant inward channels can be observed toward the lower-right region, where the local permeability is high, similar to what has been shown in Fig. 6. Sandwiched by these two dominant inward-moving channels, there exists a thicker and faster-growing outward-moving finger.

Another facet of the patterns that arise under large correlation length circumstances for $A = 0.76$ is the uneven development of fingers. For the cases in which the correlation length is much smaller than the characteristic length scale of the flow field (i.e., the unit radius of the initially circular rotating droplet, $R_0 = 1$), the permeability heterogeneity is more evenly distributed within the domain (see, for instance, the case for $l = 0.08$ in Fig. 6). In this situation, all fingers (both inward- and outward-moving ones) evolve radially, without preferred orientation. In contrast, if the correlation length is comparable to the droplet dimension, as in the cases of $l = 0.4$ and 0.8 , then the droplet interface would present regions with great permeability variations. In these cases, the portions of the droplet interface facing higher permeability would soon develop quite vigorous growing fingers. On the other hand,

parts of the interface located at low permeability regions would show fingers evolving at a much slower pace. This asymmetric behavior results in the generation of patterns presenting two very distinct fingering fronts, as the one represented in the top row of Fig. 7 for $l = 0.8$.

The changes in the correlation length also affect the development of fingering patterns in the zero viscosity contrast case ($A = 0$), illustrated in the bottom row of Fig. 7. As in the $A = 0.76$ situation, in the $A = 0$ case one can see the formation of increasingly asymmetric patterns as the value of l is augmented. For instance, for the largest l ($l = 0.8$) one observes numerous thin fingers that evolve more evenly on the left front of the pattern that faces a region of lower permeability. On the right front, where permeability is higher, faster and longer fingers arise, in a quite explosive, visually striking fashion.

Despite the similar types of overall dynamical responses for the cases of $A = 0.76$ and $A = 0$ pictured in Fig. 7, a noticeable difference between the ultimate patterns formed is the typical lengths of the fingering structures. The finger size distribution tends to be more uniform when $A = 0$, where fluid viscosities match. This uniformity in finger size is also due to the restrained finger merging phenomenon that occurs at early times when $A = 0$. However, when $A = 0.76$ the inward-moving fingers of the less viscous fluid penetrate the more viscous inner fluid, a situation that is unstable with respect to the Saffman-Taylor instability. This viscosity-unstable inward motion, associated with local permeability heterogeneity, induces significant finger merging, resulting in more irregular interfaces.

We close this section by discussing a relevant issue. As pointed out earlier in this work, in our current numerical simulations all the data obtained for particular values of s and l use the same permeability pattern. However, ideally, for each particular value of s and l , multiple permeability distributions with different random number realizations should be performed in order to more rigorously describe the possible statistical behaviors. Unfortunately, the numerical implementation of the use of multiple permeability patterns, accompanied by repeated measurements, would require enormous effort regarding modifications in our numerical scheme. This is beyond the scope of our present work.

Even though the results presented in this work are based on a single realization, some useful, conclusive observations can still be extracted. From previous studies of fingering formation in a quarter five-spot [10] and radial injection-driven [14] configurations in heterogeneous porous media, it has been found that the sizes of the fingers are predominantly determined by the correlation lengths. On the other hand, the variance does not significantly alter the sizes of fingers but just provoke penetration toward a preferred region. Because of the random character of the permeability distributions, identical fingering patterns are not obtained, even for realizations associated with the same statistical parameters. Moreover, similar global features such as the overall fingering pattern, and the interfacial length, might be observed in different realizations associated with the same statistical parameters. By the reasons stated above, the typical size of fingers, as well as the overall morphology of the fingering patterns will not be significantly changed in permeability distributions generated

by different random realizations. These observations are supported by the repeated global measurements for interfacial lengths performed in Ref. [26], using different initial random inputs. It has been demonstrated [26] that the interfacial lengths remain nearly unaltered for the same control parameters, regardless their initial random inputs. Nevertheless, it has also been verified that, local quantitative measures, such as the positions of the outmost and innermost fingertips, r_f , might become inconclusive for different random distributions. In this case, a dominant finger usually evolves more rapidly, and even can form a channel, for a certain distribution in which the region of high permeability aligns along such a finger [10,14]. In any case, all these facts indicate that, despite its limitations, our current numerical approach is useful to capture important general features of the pattern formation process in rotating 2D heterogeneous porous media.

IV. SUMMARY AND CONCLUSION

There are plentiful examples of studies addressing the formation of fingering patterns for effectively 2D flows in a rotating Hele-Shaw cell, a device equivalent to a 2D rotating homogeneous porous medium. In this work, we revisited this suggestive pattern-forming problem but considered fluid displacement in a rotating heterogeneous porous medium. We utilized advanced numerical simulations, and investigated the development of rotationally induced fingering instabilities that arise in a 2D heterogeneous environment, by considering a log-Gaussian distribution characterized by a variance s and a correlation length l . Both s and l are coupled with different dimensionless parameters of the problem, including the viscosity contrast A and surface tension-related Galileo number Ga . In this framework, changes in permeability magnitude are determined by the variance, while the correlation length prescribes the typical size of more permeable regions.

Our numerical results indicate that, in general, the presence of permeability heterogeneity has a significant impact on the pattern-forming dynamics. First, it has become clear that permeability heterogeneity introduces additional perturbations into the system, so the onset of fingering formation occurs much earlier than it would happen under usual homogeneous situations. In addition, we have observed that the dominant radial flow induced by centrifugal forces is actually inhibited by the randomly distributed permeability field. So, the

occurrence of finger merging phenomena is favored. This heterogeneous effect causes a reduction in the ultimate number of fully developed fingers.

By the same token, under the presence of heterogeneity, the typical finger shapes appear more irregular, presenting thicker roots, and slim bodies near the finger tips. Such slim fingers frequently go through a permeability-induced pinch-off process, giving rise to isolated satellite droplets and small finger segments and resulting in patterns that look quite fragmented. Additionally, we have found that permeability variation favors the development of long and fast-moving fingers, and, consequently, finger competition among the growing structures is enhanced under heterogeneous conditions.

Most of these qualitative observational conclusions have been checked and substantiated by more quantitative measurements extracted from the time evolution of two useful auxiliary quantities: the interfacial length L and the maximum penetration fingertip position r_f .

During the analysis of the general morphological features summarized in the previous paragraphs, we had the opportunity to identify the most emblematic effects induced by the governing heterogeneity parameters s and l . First, we have deduced that the variance of the heterogeneity field s plays a more important role regarding the local fingering phenomena. In other words, larger values of s tend to increase finger competition and favor finger merging and finger pinch-off. The major consequence of these effects is the fact that the fingering patterns tend to be more and more fragmented as s is augmented. On the other hand, we have found that the correlation length l has a more global effect, strongly affecting the overall shape of the fingering patterns. More precisely, our results show that larger values of l induce the formation of eye-catching, increasingly asymmetric, structures that are quite distinct from the conventional, nearly radially symmetric, patterns generated under homogeneous conditions.

ACKNOWLEDGMENTS

J.A.M. thanks CNPq (Brazilian Research Council) for financial support under Grant No. 304821/2015-2. C.-Y.C. was supported by the Ministry of Science and Technology of the Republic of China (Taiwan) under Grant No. MOST 105-2221-E-009 -074-MY3.

-
- [1] P. G. Saffman and G. I. Taylor, *Proc. R. Soc. Lond. A* **245**, 312 (1958).
 - [2] G. M. Homsy, *Annu. Rev. Fluid Mech.* **19**, 271 (1987); K. V. McCloud and J. V. Maher, *Phys. Rep.* **260**, 139 (1995); J. Casademunt, *Chaos* **14**, 809 (2004).
 - [3] L. Paterson, *J. Fluid Mech.* **113**, 513 (1981).
 - [4] L. W. Schwartz, *Phys. Fluids A* **1**, 167 (1989).
 - [5] Ll. Carrillo, F. X. Magdaleno, J. Casademunt, and J. Ortín, *Phys. Rev. E* **54**, 6260 (1996).
 - [6] E. Alvarez-Lacalle, J. Ortín, and J. Casademunt, *Phys. Fluids* **16**, 908 (2004).
 - [7] J. A. Miranda and E. Alvarez-Lacalle, *Phys. Rev. E* **72**, 026306 (2005).
 - [8] R. Folch, E. Alvarez-Lacalle, J. Ortín, and J. Casademunt, *Phys. Rev. E* **80**, 056305 (2009).
 - [9] C.-Y. Chen, Y.-S. Huang, and J. A. Miranda, *Phys. Rev. E* **84**, 046302 (2011).
 - [10] C.-Y. Chen and E. Meiburg, *J. Fluid Mech.* **371**, 269 (1998).
 - [11] E. Meiburg and C.-Y. Chen, *SPE J.* **5**, 129 (2000).
 - [12] H.-G. Lee, J. S. Lowengrub, and J. Goodman, *Phys. Fluids* **14**, 492 (2002).
 - [13] C.-Y. Chen, Y.-S. Huang, and J. A. Miranda, *Phys. Rev. E* **89**, 053006 (2014).
 - [14] C.-Y. Chen and P.-Y. Yan, *Phys. Fluids* **27**, 083101 (2015).
 - [15] S. L. Waters and L. J. Cummings, *Phys. Fluids* **17**, 048101 (2005).

- [16] E. Alvarez-Lacalle, H. Gadêlha, and J. A. Miranda, *Phys. Rev. E* **78**, 026305 (2008).
- [17] M. Ruith and E. Meiburg, *J. Fluid Mech.* **420**, 225 (2000).
- [18] C. T. Tan and G. M. Homsy, *Phys. Fluids A* **4**, 1099 (1992).
- [19] M. Shinozuka and C.-M. Jan, *J. Sound Vib.* **25**, 111 (1972).
- [20] J. Soriano, J. Ortín, and A. Hernández-Machado, *Phys. Rev. E* **66**, 031603 (2002).
- [21] D. Geromichalos, F. Mugele, and S. Herminghaus, *Phys. Rev. Lett.* **89**, 104503 (2002).
- [22] C.-Y. Chen and E. Meiburg, *J. Fluid Mech.* **371**, 233 (1998).
- [23] Y.-S. Huang and C.-Y. Chen, *Comput. Mech.* **55**, 407 (2015).
- [24] M. Sajjadi and J. Azaiez, *Phys. Rev. E* **88**, 033017 (2013).
- [25] C. Nicolaidis, B. Jha, L. Cueto-Felgueroso, and R. Juanes, *Water Resour. Res.* **51**, 2634 (2015).
- [26] C.-Y. Chen, C.-W. Huang, L.-C. Wang, and J. A. Miranda, *Phys. Rev. E* **82**, 056308 (2010).